Third International Conference on CFD in the Minerals and Process Industries
CSIRO, Melbourne, Australia
10-12 December 2003

COMPUTATIONAL MODELLING OF BUBBLES, DROPLETS AND PARTICLES IN METALS REDUCTION AND REFINING

M CROSS, T N CROFT, G DJAMBAZOV and K PERICLEOUS

Centre for Numerical Modelling and Process Analysis
University of Greenwich, LONDON SE10 9LS, UK

ABSTRACT

The CFD modelling of metals reduction processes particularly always seems to involve the interaction of liquid metals, a gas (often air) top space, liquid droplets in the top space and injection of both solid particles and gaseous bubbles into the bath. These phases all interact and exchange mass, momentum and energy. Often it is the extent to which these multi-phase phenomena can be effectively captured within the CFD model which determines whether or not a tool of genuine use to the target industry sector can be constructed. In this paper we discuss these issues in the context of two problems – one involving the injection of sparging gases into a steel continuous caster and the other based on the development of a novel process for aluminium electrolysis.

INTRODUCTION

Metals reduction and refining processes almost inevitably involve the controlled interaction of gaseous bubbles, liquid droplets and solid particles in the context of a liquid bath with a gas top space. Examples of relatively recent novel process developments include:

- The ISA/SIRO/AUSsmelt family of processes for the smelting of copper and a range of other ores [1,2,3]
- The HIsmelt process for the smelting of iron ores [4,5,6]
- Novel processes for the reduction of alumina [7,8,9]

The computational modelling of such processes is very complex, involving:

- NS turbulent multi-component fluid dynamics with free surfaces
- The injection of gaseous bubbles (or clusters) into the bath, the ejection of liquid droplets into the air top space and the injection of solid particles
- Heat transfer amongst all the materials present
- Chemical reactions amongst all the phases present

There are further problems of both time and length scale in these problems:

- At the elevated temperatures these processes operate at, the chemical reactions are controlled primarily by transport of species and, usually, rates can be considered to be instantaneous
- The particulate/droplet/bubble flow dynamics are of the order of sub-seconds
- The timescale of the bath stirring processes are many minutes
- The time scale of the reduction/refining process is hours

There are a range of genuine challenges in the problems that the analysis of these processes throws up. For example, it is not that the detailed description of turbulence is unimportant, it is more that there are many other factors that control the transport aspects of the process. As such, in considering each aspect of the process it is only worth modelling in fine detail to the extent that other aspects of the process can be captured. CFD technology is founded upon the context that the fluid phase can be considered as a continuum. Where there is more than one fluid present, typically as a gas and a liquid metal mixture, then each of these is considered as a component of a heterogeneous fluid with variable properties.

In this paper we describe two approaches to capturing the behaviour of bubble/ droplet/ particulate (BDP) systems in the context of a multi-component reacting fluid which is subject to thermal, electric current and turbulent forces, and illustrate their use in the modelling of two reduction/refining processes.

COMPUTATIONAL MODELS OF FREE SURFACE FLUIDS WITH BUBBLES/DROPLETS AND PARTICLES

The simulation process models all consider the solution domain as a continuum which is a mixture of liquid/solid metal, and possibly other fluids, such as, molten flux and/or air), and some or all of solid particles, liquid droplets and gaseous bubbles. The system is modelled as a single liquid with a variety of components, which may well have different densities and other physical/thermal properties. Phase change is modelled through a source-based method. The position of the interface between the metal and the molten flux is predicted using a free surface procedure. A cell centred finite volume method is used to discretise the governing equations on an unstructured mesh and the resulting linear systems are solved iteratively using a derivative of the SIMPLEC procedure and the simulations reported here were all achieved within the multi-physics simulation toolkit PHYSICA [10]. The equations used are described in the remainder of this section.

Continuum equations of thermo-fluid behaviour

The conservation equations for momentum and mass for three dimensional fluid flow expressed in vector notation are

$$\frac{\partial}{\partial t}(\rho \underline{u}) + \nabla.(\rho \underline{u}\underline{u}) = \nabla.(\mu \nabla \underline{u}) - \nabla p + \underline{S} \quad (1)$$

$$\frac{\partial \rho}{\partial t} + \nabla.(\rho \underline{u}) = 0 \quad (2)$$

where $\underline{u}$ is the velocity vector, p is the pressure, ρ is the mixture density and μ is the effective viscosity. When modelling turbulent effects the turbulent viscosity is calculated through the solution of a standard k-ε model. The source vector in the momentum equation, $\underline{S}$, includes the body forces, such as buoyancy, boundary effects and for solidification problems the Darcy source. The Darcy source represents the resistance to flow resulting from the presence of solid and is equal to

$$\frac{\mu}{K}\underline{u} \quad (3)$$

where K is the permeability calculated here using the Carmen-Kozeny equation

$$K = \frac{f_L^3}{\zeta (1 - f_L)^2} \quad (4)$$

f_L is the fraction of liquid and ζ is constant associated with the mushy region.

The energy equation, with temperature as the dependent variable, is given by

$$\frac{\partial}{\partial t}\left(\rho c_p T\right) + \nabla.\left(\rho c_p \underline{u} T\right) = \nabla.\left(k \nabla T\right) + S_T \quad (5)$$

where k is the thermal conductivity and c_p is the specific heat. The source term, S_T, contains the contributions from the boundaries and the effects of phase change. The energy released due to a change of phase can be expressed as

$$S = -\frac{\partial}{\partial t}\left(\phi \rho_m f_L L\right) - \nabla.\left(\phi \rho_m \underline{u} f_L L\right) \quad (6)$$

where L is the latent heat of solidification, ρ_m is the density of the metal and ϕ is the fraction of metal obtained from the free surface model.

The interface between the molten flux and the liquid metal is modelled using the scalar equation [11]. The algorithm solves the equation

$$\frac{\partial \phi}{\partial t} + \underline{u}.\nabla \phi = 0 \quad (7)$$

for the metal volume fraction in an element, ϕ, on a stationary mesh. Smearing of the interface is reduced significantly by solving equation (7) explicitly and using a van Leer advection scheme. The continuity equation (2) is adjusted to provide an equation that represents volume conservation

$$\frac{D(\ln \rho)}{Dt} + \nabla.(\underline{u}) = 0 \quad (8)$$

where D/Dt is the substantial derivative. Expressing the equation in this form removes the problems caused by the density discontinuity at the interface.

Modelling the interaction of bubbles/droplets and particles with fluids

The solution of multi-phase flows has engaged the attention of many workers over three decades. In most of the early work which involved combinations of Lagrangian particle tracking and Eulerian continuum fluids, as above, it was generally assumed that the particulate phase was highly disperse and so the coupling was only one way – that is the flow field influenced the Lagrangian, particles but not *vice versa*. However, in the 1970's Spalding developed the IPSA approach to model two inter-dispersed continuum fluid phases [12]. This method had the key advantage of ensuring that the full coupling between both fluid phases was accounted for and this enabled the behaviour of multi-phase fluid systems including heat and mass transfer, e.g. combustion, to be addressed. Although IPSA has been used with some success, for example, by Schwarz [13,14] in modelling the highly turbulent liquid bath of the HIsmelt process, in most cases IPSA is not the most cost effective means of representing the interaction amongst 'particulates' and continuum fluids. However, there are now other schemes which are both more physically intuitive and enable full coupling between continuum fluid and 'particulate' phases. We describe two of these below and illustrate their use in metals processing applications.

Bubble/Droplet/Particle modelling 1:- Particle Tracking Scheme

The particle-tracking model uses a novel approach, which was originally developed to model liquid metal droplets in an iron converter [15], to couple the influence of a flux of particles to the mean flow of the fluid through variation in the density field. The B/D/P is split into a number of packets each representing an equal mass such that the total mass of all packets equals the required inflow rate. One particle is tracked for each packet using a conventional Lagrangian method. The particle velocity, U_p, is computed from

$$U_p = (U_p + S_u * \delta t)/(1 + F * \delta t) \quad (9)$$

where

$$F = 0.75\, C_d \rho V_{slip}/\left(d_p \rho_p\right),$$
$$S_u = F U_p + \left(\rho_p - \rho\right) g / \rho_p,$$
$$V_{slip} = U_p - U.$$

Here the subscript p indicates particle values, other values are those associated with the metal, d_p is the diameter of the particle and g the gravity. The particle time step size, δt, is chosen so that a particle takes a specified number of steps to cross an element. Two methods were used to calculate the drag coefficient C_d. The first of these methods [16] is suitable for small bubbles that remain spherical in shape. The method, which has been used in many models including [17], uses the equation

$$C_d = \frac{24.0}{Re}\left(1+0.15\,Re^{0.687}\right)+\frac{0.42}{\left(1+\frac{42500}{Re^{1.16}}\right)} \quad (10)$$

The method is appropriate for small bubbles (< 1mm) in contaminated fluid, or fluid containing surfactants. An alternative method [18], that assumes a non-rigid surface, uses a range of equations dependent on the Reynolds number, Re, and the Weber number, We. These non-dimensional numbers are calculated from the equations

$$Re = d_p V_{slip}/\nu \qquad We = \rho V_{slip}^2 d_p/\sigma \quad (11)$$

where σ is the bubble surface tension and ν is the laminar viscosity. The equations associated with the method are

$$\begin{aligned} C_{d0} &= 16/Re && Re<0.49 \\ C_{d0} &= 20.68/Re^{0.643} && Re\le 100 \\ C_{d0} &= 6.3/Re^{0.385} && We\le 8, Re\le \frac{2065.1}{We^{2.6}} \\ C_{d0} &= We/3 && We\le 8, Re>2065.1/We^{2.6} \\ C_{d0} &= 8/3 && We>8, Re>100 \end{aligned} \quad (12)$$

The second of the above equations is the dirty water expression of Wallis [19]. The drag coefficient for this method is calculated using

$$C_d = C_{d0}\,(1-V_{ar})^{-1.7} \quad (13)$$

where V_{ar} is the volume fraction of the B/D/P swarm. The multiplier of C_{d0} in the above equation, termed the swarming coefficient, accounts for the reduction in drag due to B/D/P-B/D/P interactions.

The particles are randomly seeded just inside the inlet area. Particles are assigned an initial velocity, close to the continuum velocity, and tracked until they reach some kind of fluid boundary(which could be for example a metal-flux interface or solidified metal). The time a particle spends in an element, Δt, is recorded and the B/D/P volume fraction of the element is increased by

$$\Delta t\,(\dot{m}_{ar}/N_p)/\rho_p \quad (14)$$

where $\dot{m}_{ar}$ is the mass flow rate of gas at the inlet and N_P is the number of packets. This volume fraction and its associated momentum is then added back into the continuum equations for the host fluid. The energy associated with the B/D/P is also added as a source term back into the thermal equation as well. In this way the B/D/P phase is fully coupled in with the host fluid phase with respect to mass, momentum and thermal energy conservation.

Bubble/Droplet/Particle modelling 2:- Continuum approach

When considering the motion of bubbles in liquid, it is convenient to take advantage of the fact that the bubbles have virtually no inertia; of course, the same is not true for solid particles, and then a decision has to be taken whether to ignore their inertia or not. In the absence of inertial forces, the lift experienced by a bubble due to density difference is equal in magnitude and opposite in direction to the drag caused by the liquid [16]:

$$(\rho_{liq}-\rho_{bub})V_{bub}g = C_d\rho_{liq}\frac{V_{slip}^{\ 2}}{2}A_{bub}.$$

Where V_{bub} is the volume and A_{bub} is the surface area of the bubble. Under the assumption that the bubbles retain their spherical shape at all times, see above, then the drag coefficient of small rigid particles may be used [16]. The Reynolds number has to be calculated based on the particle/bubble diameter and the particle *slip velocity*. If the bubble diameter is prescribed on the basis of experimental observations, the slip velocity can be determined implicitly from the above equation by simple iteration – usually it takes less than 10 iterations to converge.

The slip velocity field determined as described above is strictly vertical – if this is used directly in the simulations, bubbles will be trapped and start accumulating under any horizontal feature of the geometry. A reasonable assumption here is that the bubbles will follow the streamlines of a *potential* velocity field as they move upwards around any obstacles. The velocity potential φ can initially be resolved as a non-dimensional quantity in the particular geometry in a way that is similar to the calculation of a non-dimensional electric potential. The boundary conditions for φ can be as follows: fixed value of zero at the bottom of the vessel, fixed value of one at the top free surface and free slip on all other solid walls. After that taking the gradient of the non-dimensional velocity potential will provide the slip velocity field:

$$\vec{V}_{slip} = -k\nabla\varphi.$$

Here k is a scaling-up coefficient with the true calculated value of the slip velocity.

The greatest advantage of the slip-velocity-field approach described above is that there is no need to do time-dependent simulations and particle tracking. Instead, the bubbles can be represented as a scalar concentration variable and the general transport equation can be solved for that variable in *steady-state* mode which is computationally much less expensive. The only thing that needs to be done is to *add* the local slip velocity to the local convection velocity for the bubble concentration variable alone. This can be achieved either by modification of the code or by adding a source term, the latter method being more generic.

Applications 1:- Sparging of the submerged entry nozzle in continuous casting

In the continuous casting of steel the liquid metal flows into the concast mould from a tundish through a submerged entry nozzle (SEN) located under the liquid mould flux layer within the liquid metal pool. Argon is frequently injected into the SEN to sparge the entry point into the liquid metal pool and ensure metal continues to flow. The amounts of argon injected into the bath are

significant enough that they effect the flow dynamics of the liquid metal in the region of the concast mould.

The ultimate objective of the work reported here is to develop a complete model of continuous casting which tracks the metal from its delivery into the concast machine until its exit as a solid bloom or slab. This truly multi-physics process involves multi-component multi-phase fluid flow, heat transfer with phase change, electromagnetic fields and non-linear solid mechanics. Here we will focus upon the impact of the argon bubbles in the neighbourhood of the concast mould. The details of the full flow based part of the model are described by Pericleous et al [20]. The model captures the liquid metal flow into the mould, the multi-component nature of the turbulent continuum fluid in the mould (i.e. liquid metal, liquid mould flux and air), the free surfaces between each of these components, the heat transfer and solidification/melting phase change, plus the behaviour of the argon bubbles clusters within the context of the fluid flow field and their impact upon the host continuum fluid. The behaviour of the argon gas injected reported here is captured through the first of the model approaches described above.

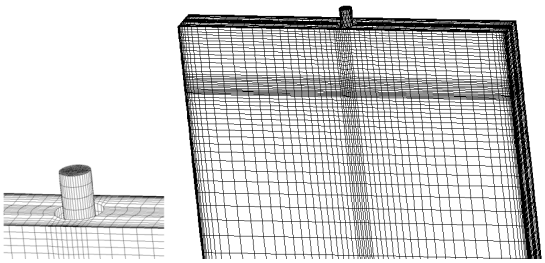

Figure 1: Mesh

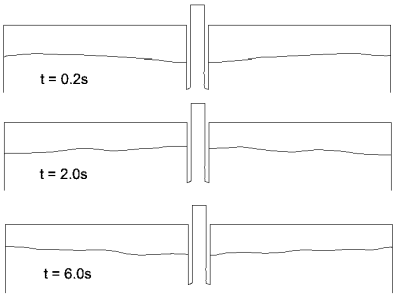

Figure 2: Interface Position

In the simulations presented here the casting velocity was set at 1.25 m/min and the flow rate of argon was 10 l/min. Figure 1 shows part of the unstructured mesh used in the simulation. The domain represents a slab with a 2.2m by 0.22m rectangular cross section and extends 5m from the meniscus. The mesh consists 150K elements including a mixture of brick, wedge, pyramid and tetrahedral elements. Figure 2 shows the flux-metal interface position at times 0.2s, 2.0s and 6.0s. A number of wavelengths are evident from the figures, and we suggest that a Fourier analysis of the results would help explain the nature of this wave action. For the initial simulations reported here equation (10), was used; this assumes that bubbles remain spherical and behave like rigid bodies, and is not necessarily true for the bubble sizes modelled here. However, this simplified form has served a useful role in scoping the issues to be resolved with further work.

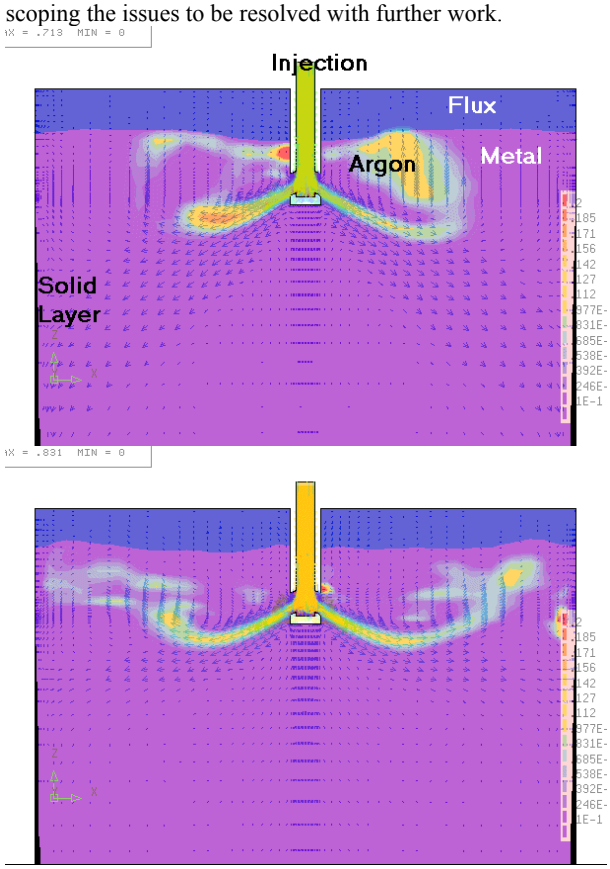

Figure 3: Contours of Argon Concentration

Figure 3 is a combination plot showing the instantaneous flux-metal interface, contours of argon volume fraction and velocity vectors at two time steps taken from a 25 frame animation. Also shown for reference is the solid skin region, taken from a steady-state simulation. A single bubble size, of 1mm diameter, was modelled. Large values of argon concentration appear at the jet exits from the nozzle ports in an alternating fashion. This bubble concentration may be a consequence of the well-type bottom of the nozzle which tends to create a stagnation region inside the nozzle. It is possible that coalescence would occur here under these conditions. The large concentrations leads to asymmetry in the flow due to the strong localized buoyancy force. For this bubble size (and C_d assumption) most bubbles flow upwards towards the interface. Their lateral spread into the slab seems to be time dependent. It is also observed that high gas concentrations near the interface are accompanied by a wave crest. These simulations have acted as a stimulus to further research to determine whether this is a cause or effect and, if the former, how to control its behaviour to minimise the generation of such surface waves.

Applications 2: Low temperature slurry-electrolyte alumina reduction cells

Conventional Heroult-Hall technology is the core technology used in the smelting of aluminium. It is exploited across the world and has been the focus of considerable research and development efforts over a number of generations. In parallel with this effort has been

various sporadic research programmes targeted at developing alternative alumina reduction processes which are both more efficient and do not give rise to the considerable wear and replacement cost of cell anodes that is a feature of the Heroult-Hall cells. One such effort has been pursued by Brown[8,9] building upon the ideas of Beck[7]. The objective here is to develop a process that uses dimensionally stable anodes, which means that the gas evolved at the anode is oxygen rather than carbon dioxide. The alloy anodes used in this work will degrade quickly in conventional high temperature baths and so an acidic composition of sodium fluoride (NaF) and aluminium fluoride (AlF_3) is used as the electrolyte, at about its eutectic composition, because here the melt temperature is about 695^{o}C. The process can then run around 750^{o}C without causing undue wear on the anodes. Unfortunately the low temperature electrolyte bath alone is not sufficient to prevent catastrophic corrosion unless it is kept supplied with a constant source of dissolved alumina. At 750^{o}C alumina solubility is low, so low that the even at saturation, diffusion of dissolved alumina to the anodes in the system will not support a sufficiently high current density for the reduction process to operate effectively. Brown addresses this issue by the use of a slurry electrolyte of un-dissolved alumina particles which act as a source of dissolved alumina in the bath to supplement its loss through transport to and reaction at the anode.

A schematic diagram of the process is presented in Figure 4. The granular raw material is continuously introduced by a feeder located at a suitable spot above the bath surface. As it slowly dissolves, primary negative complex ions are formed in the bath. They eventually reach the anode surface and react, losing electrons and producing oxygen gas bubbles. The rising gas bubbles initiate flow in the bath due to the drag force between the gaseous and the liquid phase. As a result of the anode reaction, an intermediate solid product is formed which readily dissolves in the bath producing secondary ion complexes. Those are carried by the flow around the vessel, and on reaching the cathode surface they react by accepting electrons, releasing the product which sticks to the cathode and restoring the bath ionic composition. The liquid product accumulating on the cathode is slightly more dense than the bath; as such, droplets are formed which detach and fall to the bottom of the electrolysis cell from where the product is periodically removed by tapping. The feeder solid particles are denser than both the bath (by a factor of two) and the liquid product on the bottom of the vessel. If it was not for the electrolyte flow, they would sink to the bottom and be prevented (by the product lying there) from further dissolution thus piling up and clogging the cell. However, the incoming particles are sufficiently small to be influenced by the flow and they become even smaller as they dissolve. This means that, if the process is tuned correctly, all particles can be completely dissolved before being able to settle on the bottom.

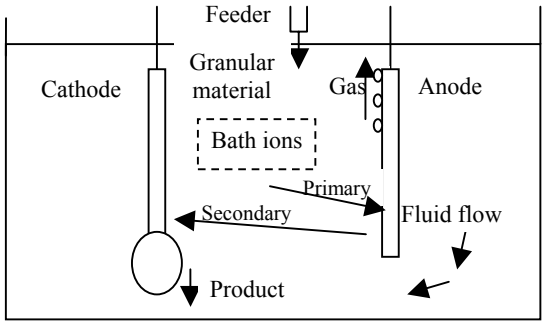

Figure 4: Schematic diagram of electrolysis process

The need to optimise the above aspects of the process has initiated a programme to model the new cell design. The movement of both the alumina particles and the oxygen bubbles is modelled using the Eulerian approach highlighted above. The justification for this approach is that they are both very small – the oxygen bubbles clearly have no inertial forces of their own, and single particle experiments with the Lagrangian model (described above) demonstrated that the alumina particles also had a negligible acceleration due to their own mass. The full model involves:

- Prediction of a turbulent electrolyte flow field and the representation of a range of transported variables,
- Calculation of the electric field potential and the electrolysis current
- Specific representation of the dissolving alumina particles and the oxygen bubbles
- Calculation of the thermal field together with the solidification/melting of alumina-fluorides

Such a model is under development; the model is primarily run in the steady state and uses the second of the above models for predicting both the oxygen bubble and the alumina particle transport. In Figure 5 we show some plots of the oxygen induced flow and the distribution of the dissolved alumina for a 10A laboratory vessel [8]. What is clear here is that the rate of dissolution of the alumina particles in the melt is sufficient that the electrolyte is always at the level of saturation and so that the reaction of the alumina at the anode is not inhibited. The next objective with this work is to ensure that in the scale-up of this process to a rather larger pilot plant, the design of the equipment facilitates the continued saturation of the dissolved alumina in the electrolyte bath. As the scale of the process increases then the issues of dissolution rate, consumption at the anode and transport in the vessel become more challenging.

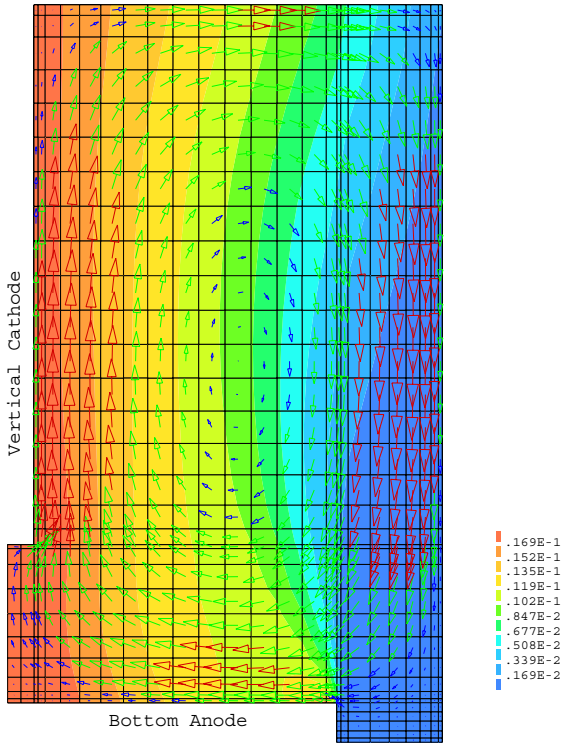

Figure 5: Contours of oxygen bubbles volume fraction

CONCLUSION

CFD modelling of reduction and refining processes in metallurgical processing always involves the interaction between:

- continuum fluids which themselves will involve a two phase system with liquid metal and cover gases, which therefore involves the capture of a free surface and
- one or more of solids, fluids and gases in particulate, droplet or bubble form.

In this work we have presented a Lagrangian-Eulerian and an Eulerian-Eulerian approach to the representation of particulates interacting with continuum fluids that are amenable to hosting a comprehensive model of reduction/refining processes involving all aspects of the heat transfer together with phase change, chemical reactions and any electromagnetic field effects. The models described here should be reasonably standard features of commercial CFD codes that target the support of modelling in reduction/refining in metallurgical processing.

REFERENCES

1. SIROsmelt, see www.minerals.csiro.au
2. AUSsmelt, see www.ausmelt.com.au
3. ISAsmelt, see www.mimpt.com.au
4. DRY,R.J., BATES, P. and PRICE, D., (1999) HIsmelt, the future in direct ironmaking, *Ironmaking Conference Proceedings*, pub ISS, pp. 1-6
5. BATES, P. AND COAD, A., (2000) HIsmelt, the future in iron-making technology, *Proceedings of 4th European and Ironmaking Conference*, **2**, pgs 597-602
6. HIsmelt, www.hismelt.com.au
7. BECK, T. R., A non-consumable anode for production of aluminium with low temperature fluoride melts, in *Light Metals*, pub TMS, 355-360 (1995)
8. BROWN, C. W., (1998) The wettability of TiB2-based cathodes in low temperature slurry electrolyte reduction cells, in *Jnl of Metals*, pp. 38-40
9. BROWN, C.W., (2000) Laboratory experiments with low temperature slurry electrolyte alumina reduction cells, in *Light Metals*, pub TMS, pp. 391- 396
10. PHYSICA, see www.multi-physics.com
11. PERICLEOUS, K.A., CHAN, K. .A., and CROSS, M., (1995) "Free surface flow and heat transfer in Cavities: the SEA algorithm", *Numerical Heat Transfer, Part B*, **27**, 487-507
12. SPALDING, D.B., (1980) Numerical computation of multi-phase flow and heat transfer, in *Recent Advances in Numerical methods in Fluid Mechanics*, C. Taylor et al (eds), Pineridge Press, pp.139-168
13. DAVIS, M., CROSS, M., PERICLEOUS, K.A. AND SCHWARZ, P., (1998) Mathematical Modelling Tools for the Optimisation of Direct Smelting Processes. *Applied Math Modelling,* **22**: 921-940
14. SCHWARZ, P., (1996) Simulation of gas injection into liquid metal melts, *Applied Math Modelling*, vol 20, pp. 41-51
15. CROFT, T.N., (1998) Unstructured mesh-finite volume algorithms for swirling, turbulent, reacting flows, *Ph.D. Thesis*, University *of* Greenwich
16. CLIFT, R., GRACE, J.R. and WEBER, M.E. (1978) *Bubbles, drops and particles*, (Academic Press)
17. SIMONIN, O. et al. (1993) "Eulerian prediction of the fluid/particle correlated motion in turbulent two-phase flows", *Applied Scientific Research*, **51**, 275
18. KUO, J.T. and WALLIS, G.B., (1988), "Flow of bubbles through nozzles", *International Journal of Multiphase Flow*, **14**, 547
19. WALLIS, G.B., (1974), "The terminal speed of single drops or bubbles in an infinite medium", *International Journal of Multiphase Flow*, **1**, 491
20. CROFT, T.N., PERICLEOUS, K.A., BOBADILLA, M. and GARDIN, P., (2003) Three-phase dynamic modelling of the continuous casting process, MCWASP Proceedings